MICHIGAN STATE
UNIVERSITY

National Superconducting Cyclotron Laboratory

THE PROGRAM LISE: A SIMULATION OF FRAGMENT SEPARATORS

D. BAZIN, O. TARASOV, M. LEWITOWICZ, O. SORLIN

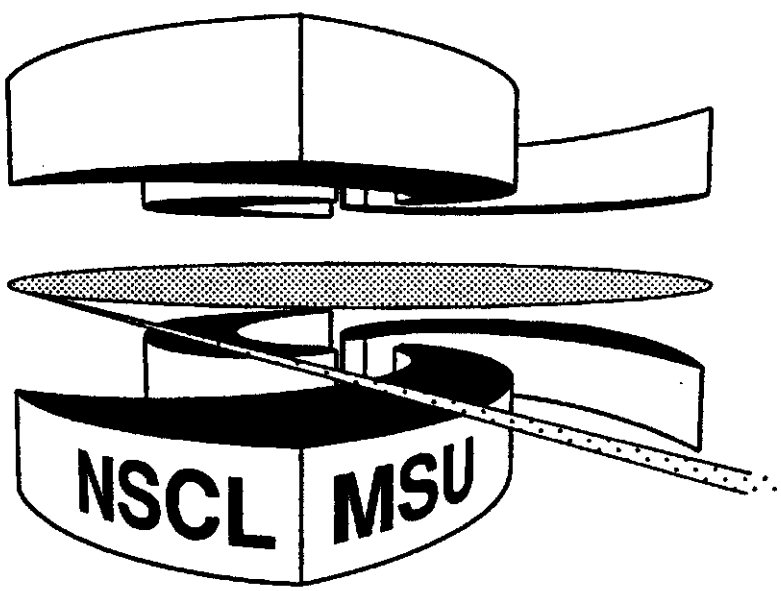

MSUCL-1187

JANUARY 2001

The program LISE: a simulation of fragment separators

D. Bazin [a] O. Tarasov [b,c] M. Lewitowicz [c] O. Sorlin [d]

[a] *National Superconducting Cyclotron Laboratory, Michigan State University, East Lansing, MI 48824-1321, USA*

[b] *Flerov Laboratory of Nuclear Reactions, Joint Institute for Nuclear Research, 141980 Dubna, Moscow region, Russia*

[c] *Grand Accelérateur National d'Ions Lourds, BP 55027, 14076 Caen Cedex, France*

[d] *Institut de Physique Nucléaire, BP 1, 91406 Orsay Cedex, France*

Abstract

This paper is a description of the program LISE which simulates the operation of fragment separators used in the production of radioactive beams via fragmentation. The various aspects of the physical phenomenons involved in the production of such radioactive beams are discussed. They include fragmentation cross sections, energy losses in materials, ionic charge state distributions, as well as ion optics calculations and acceptance effects. Among the goals of this program is a highly user-friendly environment, designed not only to forecast intensities and purities for planning future experiments, but also as a tuning tool during experiments where its results can be quickly compared to on-line data. In addition, several general purpose tools such as a physical parameters calculator, a database of nuclei properties, and relativistic two body kinematics calculations make it also attractive in experiments where radioactive beams are not involved. After a general description of fragment separators, the principles underlying the calculations are presented, followed by a practical description of the program and its many features. Finally, a few examples of calculations are compared to on-line data, both qualitatively and quantitatively.

Key words: Fragment separator, radioactive ion beams, beam optics, projectile fragmentation, phase space distributions
PACS: 25.70.M, 41.85, 07.05

Email address: bazin@nscl.msu.edu (D. Bazin).

1 Introduction

1.1 History

The conception of the program LISE was elaborated during the first experiments performed on the fragment separator LISE [1] in the mid 80's. The aim of these experiments was the production of light drip-line nuclei never observed before. The method of production was the then newly applied projectile fragmentation in which nuclei accelerated to energies several times above the Coulomb barrier randomly breakup on a fixed target. The resulting fragments were then separated in magnetic rigidity by means of two dipoles, so that drip-line nuclei would be observed in the focal plane. From the beginning it appeared necessary that some calculations had to be done before the experiments in order to predict the magnetic rigidity at which a specific fragment would be observed. These calculations had to simulate not only the initial conditions of the experiment (beam energy, target thickness ...), but also the fragmentation process itself. It was quickly realized that such a tool should also be highly interactive, so that immediate results from the calculations could be compared to data acquired on-line.

As new and improved methods of selecting the interesting fragments were invented, the program LISE evolved accordingly. The two most important steps were the adjunction of further fragment selection by energy loss in a wedged material, and the use of a velocity filter, later followed by a small dipole to compensate for the dispersion and hence obtain mass separation. The resulting secondary beam of fragments could then be made nearly 100% pure, at least for light nuclei ($A < 20$). The appelation Radioactive Nuclear Beam (RNB) was then coined to designate such beams, and a wide range of new experiments and prospects opened to study nuclear matter far from stability using them.

1.2 Purpose

Nowadays, projectile fragmentation is being used worldwide in many laboratories to produce Radioactive Nuclear Beams. Being able to predict as well as identify on-line the content of RNBs is therefore of prime importance. This has guided the definitions of the main purposes and characteristics of the program:

- Predict fragment separator settings to obtain a specific RNB.
- Predict the intensity and purity of the chosen RNB.
- Simulate identification plots to be compared on-line.
- Provide a highly user-friendly environment.

- Possibility to configure the program for different fragment separators.

One of the main emphasis in the design of the program is to be easily learned, so that new users are able to get results for a prospective experiment very quickly. At the time the program was conceived, this requirement seemed to point towards the use of Personal Computers, which were then just starting to appear.

1.3 Platform

The deliberate choice of Personal Computers (PCs) to implement the program was made for two reasons:

- make use of user-friendly features (menus, etc...)
- being able to use the program in different laboratories worldwide without need for system adaptation

One of the drawbacks of this choice was the computing speed at the time, but nowadays this argument has vanished as CPU speed in PCs has become comparable to that of regular computers. The first versions of the program LISE were written for the Disk Operating System (DOS) of Microsoft^{TM} in the language C++. Since a few years ago, it has been transported to the Windows^{TM} environment, which is the platform of the last version (4.11). With the advent of the World Wide Web, it has become very easy to maintain and update the program, and it can now be freely downloaded and installed at the following Internet addresses: www.nscl.msu.edu/~bazin/LISE.html, dnr080.jinr.ru/lise.html and www.ganil.fr/LISE/proglise.html.

2 General description of fragment separators

While existing fragment separators have different characteristics such as their acceptances and/or maximum rigidities, they are all built on the same principles and are run in basically the same way. In many cases, the purpose of these devices is the production of RNBs as pure as possible, which can be later transported to other experimental areas. However, some experiments can take advantge of having a RNB composed of different nuclei which can then be studied simultaneously. For these reasons fragment separators have to accomplish the following set of actions:

- filter the nuclei of interest from other fragments
- collect as much as possible the nuclei of interest

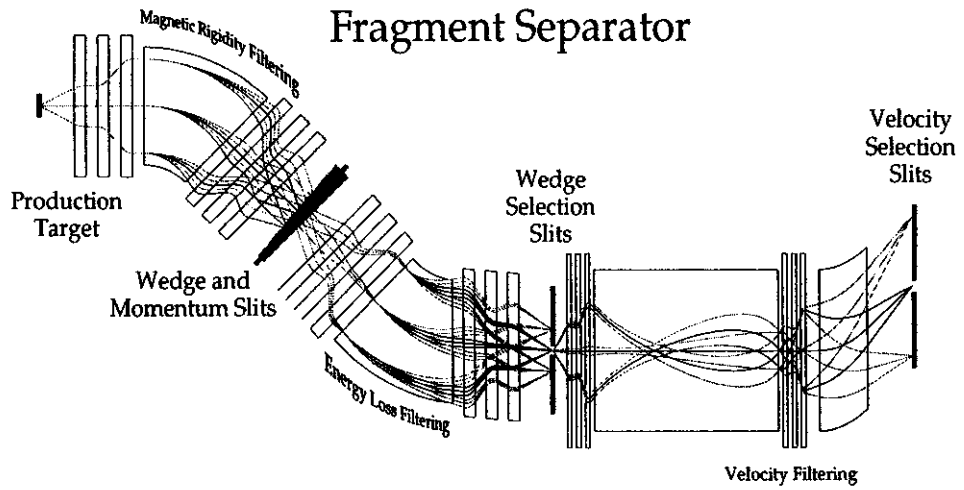

Fig. 1. Schematics of a fragment separator. The first section runs from the production target to the wedge and momentum slits, which set the momentum acceptance. The fragments selected in magnetic rigidity are then refocussed on the wedge selection slits by the second section. Finally, an optional third section operates an additional selection by using a velocity filter before the fragments are sent to a detection system, a reaction target or further beamlines.

- produce an achromatic image of the primary beam spot for further transport through other beam lines

A fragment separator is generally composed of two momentum dispersive sections mirror of each other (see fig. 1). The symmetry point between the two sections is set as a dispersive focal plane, where slits can be used to set the momentum acceptance. The second section merely compensates the dispersion caused by the first, and a one-to-one image of the beam on target can be obtained at the final focus. Because of the nuclear reactions necessary to produce the fragments of interest and of straggling in the production target, the emittances of RNBs are usually much greater than those of the primary beam. In fact, in most cases the acceptances of the separator are filled to their maximum. As a result, some transmission losses are often observed in the beamlines transporting the RNBs. Many RNBs can be produced using the two first filtering methods described in the following sections. However, depending on the mass region of interest, whether the nuclei are located close to the proton or neutron drip-lines, and on the purpose of the experiment, some RNBs need further filtering using a velocity filter.

2.1 Magnetic rigidity filtering

The first stage of filtering is accomplished by the bending elements of the first section of the separator. The magnetic rigidity of the particles (in Tm) is

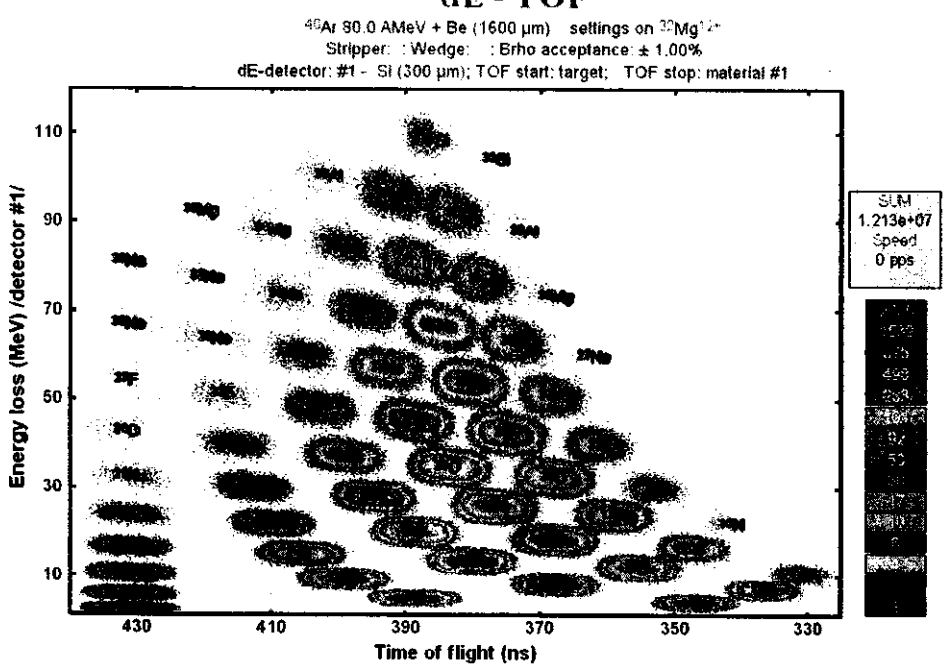

Fig. 2. Plot of transmitted fragments after magnetic rigidity filtering. The axis are the energy loss for the ordinate and the time-of-flight for the abcissa. Each fragment is labeled and the intensity is color coded. This plot and subsequent identification plots are produced by a Monte-Carlo generator to better mimic the experimental spectra observed on-line. Note that the Monte-Carlo correctly simulates the behaviour of the energy loss which decreases as the velocity increases, causing the ellipsoids corresponding to each nuclei to tilt.

related to their velocities and mass to charge ratio according to the following relativistic relation:

$$B\rho = 3.107\beta\gamma\frac{A}{Q} \tag{1}$$

where $\beta = v/c$ and $\gamma = 1/\sqrt{1-\beta^2}$ are the velocity and relativistic parameter respectively. Since fragments produced by projectile fragmentation in a thick target have very wide momentum distributions, many of them fulfill the $B\rho$ condition and are transmitted through the momentum slits. For fully stripped ions, this is equivalent to a A/Z selection. As an example, figure 2 shows an identification plot after magnetic rigidity filtering in the production of the nucleus ^{32}Mg by fragmentation of an ^{40}Ar primary beam on a Be target. Many contaminants are present and the number of ^{32}Mg nuclei only amounts to 0.25 % of the total intensity of the RNB. The optics of this first stage are usually set to a momentum dispersive focus on the wedge and momentum selection slits (see fig. 1). Some fragment separators have more than one momentum dispersive plane, allowing to place the momentum slits and wedge at different locations.

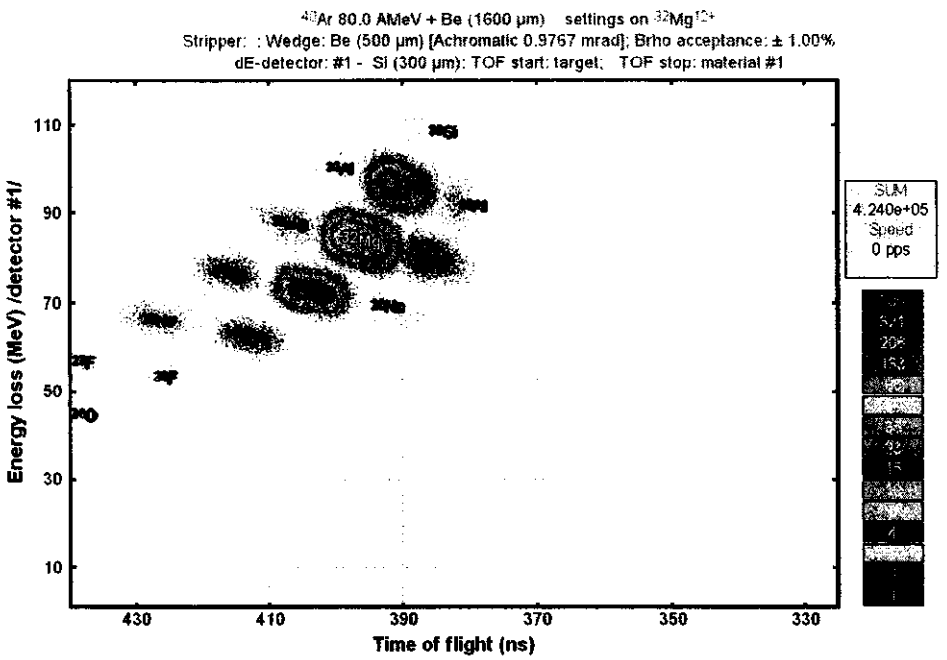

Fig. 3. Same as figure 2 but after energy loss filtering. The number of contaminants is greatly reduced due to the additional $A^{2.5}/Z^{1.5}$ selection (see text).

2.2 Energy loss filtering

The second method of filtering is based on energy loss. A material is inserted at the dispersive focal plane between the two sections of the fragment separator. Because each fragment, depending on its atomic number and velocity, looses a different amount of energy, its image at the final focus is at a different location. Using a set of slits, one can then select which fragments are transmitted. This method has been described elsewhere [1–3] and requires that the material be shaped as a wedge (or bended along a calculated curve for thin foils) in order to preserve the achromaticity of the separator. This can be simply understood qualitatively since for a given fragment different positions in the dispersive focal plane correspond to different velocities, and the energy loss must be adjusted accordingly by varying the thickness. In the program LISE this method is referred to as 'Wedge selection'. Following our example from the previous section, figure 3 shows the same plot as figure 2 obtained after energy loss filtering. The number of contaminants has been greatly reduced, and the number of ^{32}Mg nuclei now amounts to 66.4 % of the total intensity. The transmitted fragments roughly follow a $A^{2.5}/Z^{1.5}$ dependence [2]. The combined first and second sections of the fragment separator are set as an imaging system with both magnifications usually close to unity. However, to minimize the effects of straggling in the wedge, the magnification of the first section in the dispersive plane can be set to a value greater than 1, so that the second section has a magnification smaller than 1, hence reducing

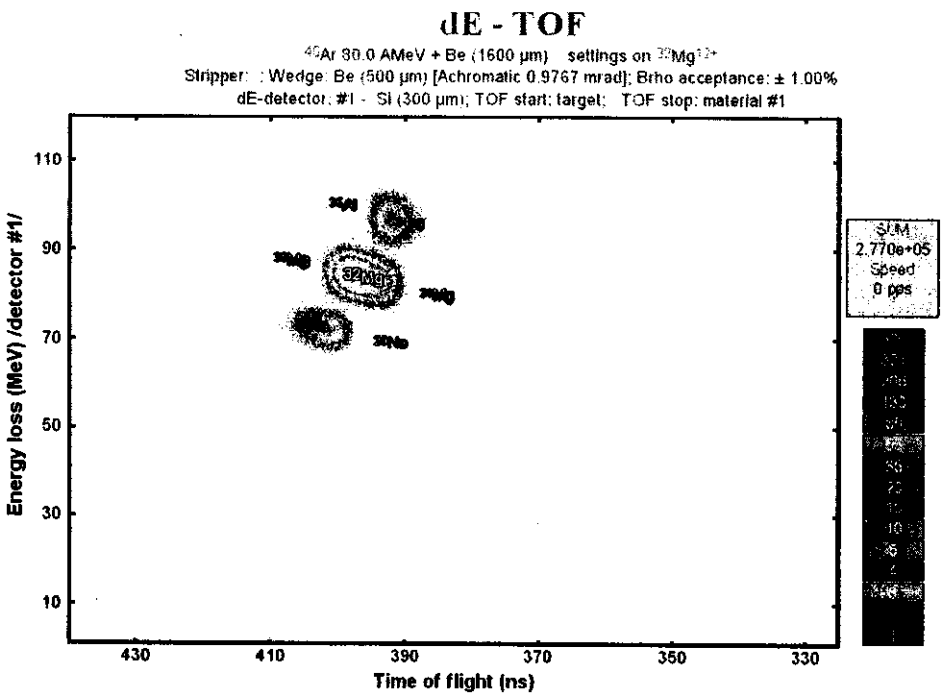

Fig. 4. Same as figures 2 and 3 but after velocity filtering.

the broadening of the image caused by the straggling in the wedge.

In some other applications, it is desirable that the shape of the wedge inserted in the beam preserves another parameter of the beam such as velocity for instance. In that case, the wedge is called monochromatic and narrows the energy and range spread of the selected particles. This feature can be used in experiments where the nucleus of interest has to be stopped in a thin solid detector or in gas. The program gives four choices of wedge profiles: homogeneous, achromatic, monochromatic and custom. For wedges made of thin foils, the program also calculates the curves for all choices of profiles.

2.3 Velocity filtering

Some experiments require a higher purity level than the one achieved with energy loss filtering. Some fragment separators have therefore added a third selection criterium based on velocity filters, also called Wien filters [4]. These devices produce electric and magnetic fields perpendicular to each other. The momentum dispersion caused by the Wien filters can be compensated for by a small dipole placed downstream. The net result is a selection in mass of the remaining fragments. Figure 4 shows the resulting identification plot, where the desired fragment, ^{32}Mg, is present at a 70.6 % level of purity. A further purification would be possible by limiting the acceptances, but at the expense of the rate.

3 Principle of calculations

The complete calculation of yields obtained on a fragment separator using projectile fragmentation involves different domains of physics. For a given ion, the yield can be written as the product of 4 independent factors:

$$\mathcal{Y} = \mathcal{I}\mathcal{N}\mathcal{F}\mathcal{A} \tag{2}$$

where $\mathcal{I}$ is the primary beam intensity, $\mathcal{N}$ the probability of producing the nucleus of interest in the target, $\mathcal{F}$ the fraction of charge Q for the given charge state and $\mathcal{A}$ the acceptances of the fragment separator. If the first factor ($\mathcal{I}$) if straightforward to calculate, the 3 others on the other hand involve nuclear reactions, atomic interactions at high velocities, and ion optics calculations. In the following subsections, we present the models used in LISE to calculate those 3 factors. As the program was intented to be a tool used during the experiments, a major emphasis was made on the speed of the calculations, which led to avoid the use of lengthy calculation techniques such as Monte-Carlo tracking simulations for instance.

3.1 Target yield

The factor $\mathcal{N}$ in eq. 2 represents the probability of producing the fragment of interest in the target. First we calculate the normalized total number of reactions $N_P(x)$ produced by a projectile P in a target slice ∂x at location x. This number is governed by the following differential equation:

$$\frac{\partial N_P(x)}{\partial x} = (1 - N_P(x))\sigma_P \tag{3}$$

where σ_P is the total reaction cross section of the projectile. With the inital condition requiring that $N_P(0) = 0$ the solution to this equation is clearly:

$$N_P(x) = 1 - e^{-x\sigma_P} \tag{4}$$

Therefore, the number of incident projectiles available at thickness x to produce the nucleus of interest F is $1 - N_P(x) = e^{-x\sigma_P}$, and $\sigma_{P\to F}$ being the cross section for producing the fragment F from projectile P , the number $N_F(x)$ of fragments F produced at thickness x follows the equation:

$$\frac{\partial N_F(x)}{\partial x} = (1 - N_P(x))\sigma_{P\to F} = e^{-x\sigma_P}\sigma_{P\to F} \tag{5}$$

The solution to this equation is:

$$N_F(x) = \frac{(1 - e^{-x\sigma_P})\sigma_{P\to F}}{\sigma_P} \tag{6}$$

which in the case of a thin target can be approximated to:

$$N_F(x) \approx \frac{(1 - (1 - x\sigma_P))\sigma_{P\to F}}{\sigma_P} = x\sigma_{P\to F} \tag{7}$$

Equation 7 is the approximation used by default in the program LISE to calculate the target yield, in which it is simply proportional to the target thickness and the cross section $\sigma_{P\to F}$. However, it becomes inaccurate when considering thicker targets and the production of very neutron-rich nuclei, as we shall see in the following.

3.1.1 One step fragmentation

As the target thickness is increased, the probability of destroying the fragment of interest just produced by projectile fragmentation becomes significant. That probability is governed by the total reaction cross section of the fragment σ_F. Taking this into account in eq. 5 leads to the following differential equation:

$$\frac{\partial N_F(x)}{\partial x} = e^{-x\sigma_P}\sigma_{P\to F} - N_F(x)\sigma_F \tag{8}$$

of which the solution is:

$$N_F(x) = \frac{e^{-x\sigma_F}(1 - e^{x(\sigma_F - \sigma_P)})\sigma_{P\to F}}{(\sigma_P - \sigma_F)} \tag{9}$$

The term $e^{-x\sigma_F}$ in eq. 9 indicates that the number of fragments produced in the target will eventually decrease as the thickness is increased, as the probability of having a second reaction destroying the previously made fragment also increases. However, this argument can be turned around: if the probability of having two successive fragmentations in the same target becomes non negligible, then many other paths to produce the final fragment of interest can open.

3.1.2 Two step fragmentation

In this process, the projectile undergoes a first fragmentation to produce an intermediate fragment i which in turn is fragmented to produce the final frag-

ment of interest F. We already know from the previous section the number $N1_i(x)$ given by eq. 9 of intermediate fragments available to make a second fragmentation at thickness x. The two step fragmentation differential equation for the path going through intermediate fragment i is therefore:

$$\frac{\partial N2_{i,F}(x)}{\partial x} = N1_i(x)\sigma_{i\to F} - N2_{i,F}(x)\sigma_F$$
$$= \left(\frac{e^{-x\sigma_i}(1-e^{x(\sigma_i-\sigma_P)})\sigma_{P\to i}}{(\sigma_P-\sigma_i)}\right)\sigma_{i\to F} - N2_{i,F}(x)\sigma_F \qquad (10)$$

where σ_i is the total reaction cross section of fragment i, and $\sigma_{P\to i}$ and $\sigma_{i\to F}$ are the cross sections to produce i from P and F from i respectively. The solution to this differential equation is:

$$N2_{i,F}(x) = (e^{-x\sigma_F}(e^{x(\sigma_F-\sigma_P)}(\sigma_F-\sigma_i) + e^{x(\sigma_F-\sigma_i)}(\sigma_P-\sigma_F)$$
$$+\sigma_i-\sigma_P)\sigma_{P\to i}\sigma_{i\to F})/((\sigma_F-\sigma_i)(\sigma_F-\sigma_P)(\sigma_i-\sigma_P)) \qquad (11)$$

and the total two step fragmentation yield is the sum of all possible paths to produce the final fragment F:

$$N2_F = \sum_i N2_{i,F} = \sum_{Z_i=Z_F}^{Z_P}\sum_{N_i=N_F}^{N_P} N2_{i,F} \qquad (12)$$

where $Z_{P,F}$, $N_{P,F}$ are the proton and neutron numbers of the nuclei involved in the reactions. Fig. 5 shows the evolution of the one, two and three step fragmentation yields as a function of target thickness for the production of ^{78}Ni from a ^{96}Zr beam (the calculation of the three step yield is given in the Appendix). The inset shows the same data in linear scale. The two and three step fragmentation become the dominant processes as the target thickness increases. Moreover, the saturation effect for the one step yield occurs at a much smaller target thickness than for the two and three step yields. This implies that, regardless of all other parameters, the total yield can be increased more in a thicker target than first thought on the basis of the one step fragmentation. This effect is especially important when trying to reach the neutron drip line, for which it is essential to limit neutron evaporation as much as possible. It is qualitatively easy to understand since the more nucleons are removed in a fragmentation, the more excitation energy the projectile-like fragment will have, and the more neutrons it will evaporate. As the cross sections reflect this behaviour, removing fewer nucleons at a time in more than one fragmentation becomes more and more favorable towards the neutron drip-line. Fig. 6 illustrates this point for the two step process in the case previously shown, the production of ^{78}Ni from ^{96}Zr. The figure shows a (N,Z) map of all possible intermediate fragments between the projectile and the final fragment. The

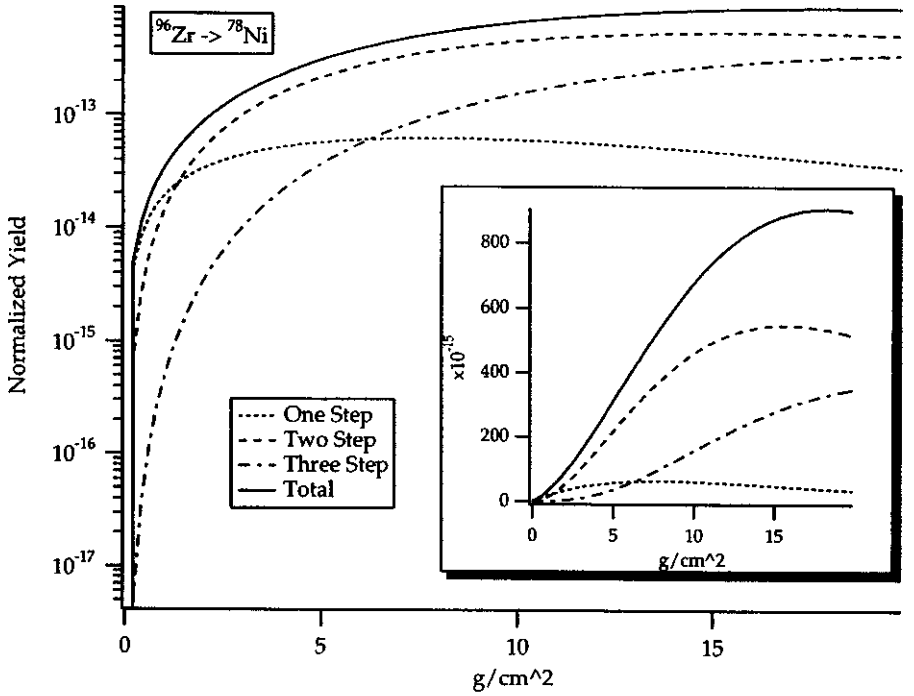

Fig. 5. Target yields as a function of target thickness for the production of ^{78}Ni from a beam of ^{96}Zr on a Be target. The inset shows the same results plotted on a linear scale for a better view of the saturation effects. The cross sections for producing the various fragments are calculated using the EPAX parametrization (see section 3.2), and the total cross sections using a simple geometric model. For thicknesses greater than 2 g/cm^2 the yield is dominated by multi step processes. This effect increases as the final fragment is chosen closer to the neutron drip-line.

size of each square represents the yield contribution of each intermediate fragment. Clearly the fragments located roughly along the straight line between the projectile and the final fragment are those which contribute the most, with an accentuated effect for the fragments with a neutron number closer to that of the ^{78}Ni. As the target thickness increases, the two "cold fragmentations" going through those intermediate fragments quickly outweight the one step process for which 12 protons need to be removed in a single reaction.

To avoid the heavy computing load involved in evaluating the analytical formulas developed above, and in order to include all multistep processes, the program LISE uses a numerical integration. At each target slice dx, the yield of each fragment i produced by secondary reactions (i.e. other than the direct - one step - fragmentation) is calculated using the formula:

$$dN_i = \sum_j^{rhombus} \sigma_{j\to i} N_j dx - \sigma_i N_i dx \qquad (13)$$

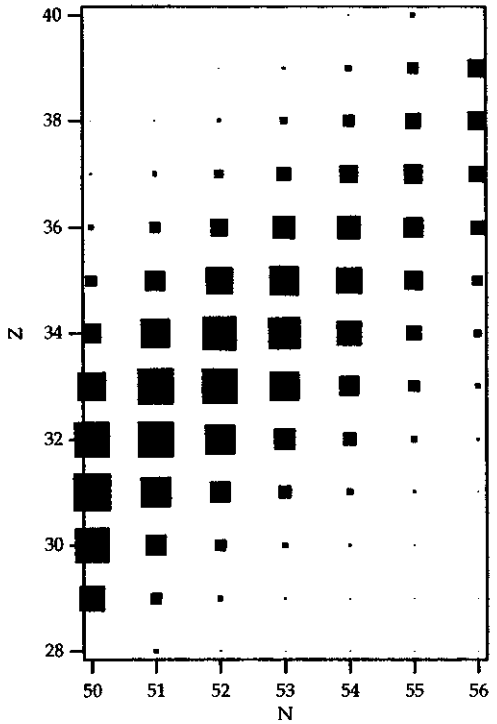

Fig. 6. Yield contributions of all possible intermediate fragments in a two step fragmentation calculation for producing ^{78}Ni from a beam of ^{96}Zr. The size of the squares is proportionnal to the yield contributions. The domain in which the important contributions are found has a rhombus shape extending from the projectile to the fragment.

with initial conditions $N_i = 0$ and $N_P = 1$, where P stands for the projectile and i for the fragments. The summation in equation 13 is limited to a rhombus domain which includes the projectile and the fragment, in order to exclude contributions from negligible secondary reactions, as illustrated in fig. 6. The contribution from secondary reactions is then added to the total yield of each fragment before the next iteration. The number of iterations can be varied and has a default value of 128.

3.2 Cross sections

In the simplest description of a fragmentation reaction, the composition of the fragments is determined by the distribution of protons and neutrons at the instant of the reaction. This would imply that the maximum cross section is found for fragments having the same A/Z ratio as the projectile, and that the distributions are energy independant above a certain total kinetic energy of the projectile (also called "limiting fragmentation" effect [5]). Indeed, it is clear from the many experiments that neutron-rich projectiles produce more neutron-rich fragments, and vice-versa. However, because the excitation

energy of the fragments is relaxed mostly via particle emission, neutron evaporation is favored due to the Coulomb barrier. This effect tends to shift the cross sections towards the proton drip line. For heavy projectiles such as ^{238}U, the energy relaxation can lead to binary fission, which favours the production of fragments closer to the neutron drip-line [6]. At intermediate energies (10 MeV/u to 100 MeV/u), it has been shown [7,8] that the projectile-target interaction time is long enough to equilibrate the A/Z ratio of the whole system (also called "memory effect"). This has led to the use of neutron-rich or neutron-deficient targets to enhance the cross section towards the drip-lines. At very high energies, the use of very thick targets can lead to multistep processes as we have seen in the previous section. Also, at energies up to a few GeV/u, Coulomb induced fission of heavy projectiles can be used to produce neutron-rich nuclei [6], although this type of reaction should not be considered as fragmentation in the nuclear sense.

The vast diversity of processes leading to the production of fragments makes it impossible to establish a single way of calculating the cross sections based on the reaction processes. Rather, an empirical approach based on experimental results seems more appropriate. This is the basis of the EPAX [9,10] parametrization which is being used in LISE. This parametrization is based on projectile and target fragmentation data and qualitatively reproduces predictions of intranuclear cascade calculations based on the Yariv-Fraenkel model [11]. Also, the parametrization reproduces around 85% of the 700 experimental fragmentation cross sections it is based on within a factor of 2. As a general rule, the parametrization is more likely to fail at greater distances from the valley of stability, where experimental cross sections are unknown, and a small error in the exponential slope of the cross section trend translates into a bigger error on the drip-line. Furthermore, it does not reproduce an effect clearly seen on experimental cross sections which is the additional binding due to the pairing of nucleons. This odd-even staggering becomes prominent at the drip-lines where only nuclei with an even number of drip-line nucleons remain bound. Consequently, the predictions of the EPAX parametrization have to be used with caution, especially on or near the drip-lines, and it is not unusual to observe differences of a factor of 5 or more with experiments. The program LISE offers the option of entering an experimentally known or better calculated cross section for any given fragment, or select previous updates of the EPAX parametrization.

As this parametrization is based on experimental data, it likely already contains contributions from the multi-step secondary fragmentation processes. However, it is very difficult to infer the amount of these contributions since the parametrization is based on data coming from numerous sources. Their effect would be a scale down of the overall yield, but wouldn't affect the qualitative conclusions given in the previous section. A more tangible approach would be to use a model such as the abrasion ablation model to calculate

the cross sections used in the calculation of secondary reactions, to avoid the interference caused by the data and take into account binding energies in a more realistic way. A first attempt aimed at the study of the production of very neutron rich nuclei using this model is under way [12].

Reactions where the final fragment has more neutrons or protons than the projectile are not covered by the EPAX parametrization. These reactions are referred to as transfer reactions, and are often used to produce radioactive beams close to the valley of stability with very high intensities. The program LISE uses and extrapolation of the EPAX parametrization to calculate the cross sections, but they should be taken with extreme caution since the actual cross sections clearly depends on the details of the reactions as well as the energy.

3.3 Fragmentation

In order to calculate the acceptance factor $\mathcal{A}$ in eq. 2, it is necessary to evaluate the phase space distributions of the fragments after having been produced in the target. A simple picture of the projectile fragmentation process used to produce RNBs is a peripheral collision which operates a sudden ablation of part of the projectile by the target [13]. The number of nucleons removed depends on the impact parameter and the emerging fragment is composed of the so-called 'spectator' nucleons. It has an intrinsic excitation energy due to its deformation and the abrasion process. The fragments then undergo a deexcitation stage by particle emission and/or γ-ray cascade. Its intrinsic momentum is determined by the contribution of each nucleon's momentum at the instant of the reaction. The fragmentation process has been studied extensively [14] and many papers have put together models to predict the characteristics of the produced fragments. For the program LISE, the most important factors are the momentum width and energy damping produced by the reaction. The momentum width directly affects the number of fragments collected in the acceptance of the fragment separator, while the energy damping lowers the energy - and therefore the magnetic rigidity (Bρ) - of any given fragment.

In an early paper [15], Goldhaber proposed a simple formula to describe the momentum width of fragments produced by projectile fragmentation. The width of the momentum distribution is given by:

$$\sigma^2 = \sigma_0^2 \frac{A_F(A_P - A_F)}{A_P - 1} \tag{14}$$

where A_F and A_P are the fragment and projectiles masses respectively, and σ_0 reflects the Fermi motion of the nucleons inside the projectile: $\sigma_0^2 = \frac{1}{5}P_F^2$. In the relativistic energy regime, the transverse and longitudinal momentum

widths of the fragments are similar. However, studies in the intermediate energy domain (10 - 100 MeV/u) [16,17] show that the transverse momentum width of the projectile-like fragments is by far greater than the longitudinal. Part of this difference can be attributed to Coulomb and nuclear deflection of the fragment by the target residue and ejected protons during the fragmentation. The following formula has been proposed to describe the perpendicular width [17]:

$$\sigma_{\perp}^2 = \sigma_0^2 \frac{A_F(A_P - A_F)}{A_P - 1} + \sigma_D^2 \frac{A_F(A_F - 1)}{A_P(A_P - 1)} \tag{15}$$

where σ_D is called the orbital dispersion, and has a typical value of 200 MeV/c. Whereas this formula is able to reproduce the data from [17] at 100 MeV/u, it fails to do so at 44 MeV/u [16]. This discrepancy can be attributed to the additional energy damping observed at 44 MeV/u, which is also responsible for the low energy tails observed on the distributions.

In the program LISE, the parallel momentum width $\sigma_{\parallel}$ can be calculated according to four different parametrizations. They are successively formula 14 from [15], a similar parametrization found in [18], the fragmentation model by Friedman [19], and finally our own parametrization [20] which uses a convolution between a gaussian and an exponential tail at low energy. This last parametrization reproduces well the data observed at intermediate energy (10 - 100 MeV/u), where dissipative effects still play an important role. The shape and width of the parallel momentum distribution directly affect the transmission through the momentum acceptance.

For the transverse momentum width $\sigma_{\perp}$, which affects the transmission through the solid angle acceptance, formula 15 is used. Both values of σ_0 and σ_D can be adjusted, with default values of 90 MeV/c and 200 MeV/c respectively.

The ratio of the fragment mean velocity to the beam velocity is directly affected by the energy damping caused by the reaction. Four different choices of calculating this ratio are also possible: it can either be held to a fixed value, or be calculated using one of the three parametrizations by [21], [22] or [20]. Some of the parameters used in these parametrizations can be modified, like for instance in [21] the amount of energy necessary to remove each nucleon from the projectile, with a default value of 8 MeV.

3.4 Phase-space distributions

To calculate the selections and transmissions of a fragment separator, the phase-space distributions corresponding to a given fragment have to be prop-

agated through its different sections. Furthermore, selection and acceptance cuts are usually performed by means of slits which are located at various image points along the device. This requires the possibility to propagate phase-space distributions from one image to another, taking into account the effect of previous cuts. Because of all those constraints, phase-space distributions can have arbitrary shapes and simplifications which occur for gaussian line-shapes for instance are not valid. A typical example is the momentum distribution of a fragment produced in a thick target, as is usually the case in a fragment separator. Whereas the distribution from projectile fragmentation is well approximated by a gaussian, the distribution which originates from the energy loss in the target on the other hand, is a Heaviside or square distribution. The combination of the two produces a "rounded edge" square-like momentum distribution which is difficult to modelize.

A standard method used to propagate such distributions is Monte-Carlo tracking simulation where the initial coordinates of the particles are sampled according to the calculated phase-space distribution, and then propagated through each element of the system [23]. For our purpose however, this method is not practical because of the computation time required for each fragment, in particular when the sampling has to cover the 6 dimensions of the whole phase-space. To remedy to this problem, we have developped a new method aimed at the fast computing of the time evolution of arbitrary phase-space distributions. The details of the method are published elsewhere [24]. It is based on the reduction of a transport integral which has the form:

$$D'(q'_1,\ldots,q'_n) = \int_1 \cdots \int_n dq'_1,\ldots,dq'_n D(q_1,\ldots,q_n) \times \prod_{i=1}^{n} \delta(q'_i - f_i(q_1,\ldots,q_n)) \quad (16)$$

where D is the initial phase-space distribution at time t and D' is the resulting phase-space distribution at time t'. The $q_1,\ldots,q_n$ and $q'_1,\ldots,q'_n$ represent the phase-space coordinates at t and t', respectively. The core of this integral is the set of functions $f_i(q_1,\ldots,q_n)$, which describe how each of the final coordinates depends on the initial ones. The Dirac δ function merely selects the combinations of initial coordinates which give a contribution at the final coordinate q'_i. In practical calculations one is more interested in the projections of the final phase-space distributions which can be reduced to:

$$P'_i(q'_i) = \int_1 \cdots \int_n D(q_1,\ldots,q_n) \times \delta(q'_i - f_i(q_1,\ldots,q_n)) dq_1,\ldots,dq_n \quad (17)$$

which can be understood as the weighted sum of the points of the distribution $D(q_1,\ldots,q_n)$ which transform into q'_i through the function $f_i(q_1,\ldots,q_n)$.

Under the assumptions of an incoherent object and first order approximation, this integral can be reduced to convolution products in the form [24]:

$$P'_i(q'_i) = \frac{1}{\prod_{k=1}^{n} R_{ik}} [\bar{P}_1 \otimes \bar{P}_2 \otimes \ldots \otimes \bar{P}_n](q'_i) \tag{18}$$

where R_{ik} are the first order coefficients which describe the transport function $f_i(q_1, \ldots, q_n) = \sum_{k=1}^{n} R_{ik} q_k$, and $\bar{P}_k(p_k) = P_k(p_k/R_{ik}) = P_k(q_k)$ with the variable change $p_k = R_{ik} q_k$. The convolution product are computed using Fast Fourier Transform techniques.

In beam optics, the phase space is usually defined in terms of the variables $(x, \theta, y, \phi, l, dp)$ where (x, θ) and (y, ϕ) are the positions and angles in the dispersive and non dispersive planes, respectively. The program LISE assumes the structure shown in fig. 1 for the fragment separator, with a focalized incoherent object at the target, dispersive focus at the intermediate image(s), and achromatic final image, meaning that the position and angle in the dispersive plane do not depend on the momentum. However, the last version (4.11) allows non-zero $(x|\theta)$ and $(y|\phi)$ terms in the matrix, meaning that focussing is no longer assumed by default. First order coefficients calculated with a beam optics program such as TRANSPORT [25] are entered in the program and can be altered interactively. This provides the possibility to simulate different devices or different optical modes of a given device.

3.5 Energy loss and stragglings

The calculation of energy loss in materials is most efficiently performed using a backward interpolation on a table of range calculations. The kinetic energy left after passing through a thickness Δx of material is equal to $E_i - \Delta E$ where E_i is the initial energy and ΔE the energy loss. If $R(E)$ is a function giving the range at a given energy E, then in terms of range one can write:

$$R(E_i) = \Delta x + R(E_i - \Delta E) \tag{19}$$

The energy loss ΔE can be calculated from a range table of the particular particle into the particular material by first interpolating on the energy to get $R(E_i)$, and then on the range to get $E_i - \Delta E$ and hence the energy loss. This method is much faster than the direct integration of the energy loss using $\Delta E = \int_{\Delta x} \frac{\partial E}{\partial x} dE$ for the same accuracy. Because it is impractical to pre-calculate range tables for all combinations of particle-material, the program LISE calculates the required tables on the fly and stores them as they occur. The range calculations are based on either the formulas by F. Hubert et al. [26,27] for heavy ions of energies from 2.5 MeV/u to 2 GeV/u in solids,

or the Hydrogen-based stopping power formulas by Ziegler et al. [28], depending on the user's choice. For very low energy particles (down to 10 keV/u), nuclear stopping corrections are added. The program also offers calculations of energy losses in gaseous materials, as well as composite materials. A list of most common composites is available from a menu, but any mixing of up to 5 different elements can be composed.

The energy straggling is calculated in MeV from a semi-empirical formula [29] based on Bohr's classical formula:

$$\delta(\Delta E) = kZ_P\sqrt{Z_T t/A_T} \tag{20}$$

where Z_P is the atomic number of the projectile, Z_T and A_T the atomic and mass numbers of the material and t the thickness in g/cm^2. The parameter k increases logarithmically with incident energy, and is parametrized from the data. Its value ranges approximately from 1 (at 1 MeV/u) to 2.5 (at 1 GeV/u).

The multiple angular straggling is determined using the formula derived in [30] where the "reduced angle" $\tilde{\alpha}_{1/2}$ follows a simple power law fitted on the experimental data:

$$\tilde{\alpha}_{1/2} = 1.00\tau^{0.55} \tag{21}$$

where τ is the "reduced thickness" expressed as $\tau = \pi a^2 Nt$ with the screening parameter $a = 0.885a_0/\sqrt{Z_P^{2/3} + Z_T^{2/3}}$ and $a_0 = 0.529 \times 10^{-8}$ cm, Z_P and Z_T the atomic numbers of the projectile and material, N the number of scattering centers per unit of volume and t the penetrated thickness. The scattering angle $\alpha_{1/2}$ is then deduced (in mrad) from the expression of the "reduced angle": $\tilde{\alpha}_{1/2} = \alpha_{1/2}Ea/2Z_P Z_T e^2$ where E is the energy of the projectile and e the electronic charge.

3.6 Charge states

Charge state distributions are important in the determination of yields as the magnetic rigidity filtering stage of the separator is sensitive on the charge of the particles (see section 2.1). *Ab initio* calculations are difficult because they require the knowledge of a huge number of cross sections and their variations as a function of energy. Better results are obtained using semi-empirical formulae fit to a set of data points. They provide a determination of the mean charge state as well as the width of the distribution. The early version of LISE used a parametrization from [31]. More recently, an extensive set of measurements has been used to determine a more accurate parametrization [32]. At low energy

(up to 6 MeV/u), the parametrization from [33] can be used. All three are available in the program.

A particularly important advantage of calculating charge state distributions becomes apparent when fragmenting heavy beams (typically from Krypton to Uranium), for which each fragment may be produced in various charge states, rather than fully stripped. In that case, the identification plots usually used become much more difficult to interpret without the help of a calculation. For instance, a regular time-of-flight vs energy-loss spectrum will show charge states of different nuclei superimposed (see section 5.1). A measurement of the kinetic energy of the fragments is necessary in order to sort out the different charge states. LISE can calculate the energy losses and ranges of the transmitted fragments in various materials, and hence simulate any particular detector setup. Then identification plots using these calculations can be produced and directly compared to on-line data during an experiment.

Another important feature about the charge state distributions is the ability to calculate their evolution as the ions go through various materials of different compositions and thicknesses. For instance, stripping foils of low atomic number (Z) are often used as a backing of high Z production targets. This has the effect of shifting the charge state distributions towards fully stripped ions in order to increase the yield on the most intense charge state. Likewise, the use of a wedge in the energy loss filtering method can modify the charge state distributions and affect the optimum setting of the second section of the fragment separator. For these reasons, the program LISE calculates the charge state distributions after every material inserted in the path of the beam.

4 Description of the program

The program includes many features which are constantly improved or added, mostly motivated by the feedback of the users. At the time of this writing, the current version is 4.11, which is the one described in this article. The purpose of this paper is not an exhaustive description of LISE and its many features. Rather, the reader is invited to obtain the program and study the extensive manual, or better yet, install it and practice by using it directly. A help is available in the program itself, and provides information on most of its features.

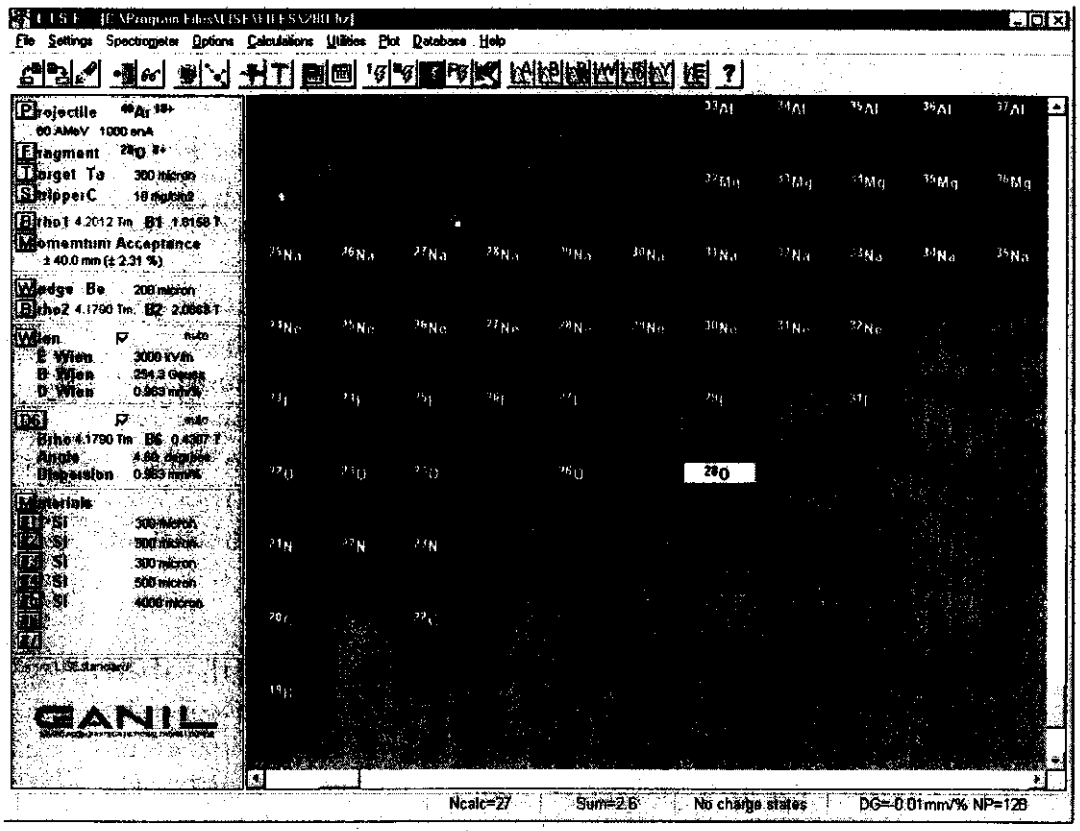

Fig. 7. Example of the main window of the program LISE. The actual window is displayed in color. The small map located on top provides shortcuts to all regions of the chart of nuclei. See text for other details.

4.1 User interface

Figure 7 shows an example of the main window of the program. The principal pane of the display is taken by the chart of nuclei, which can be scrolled in both the number of protons (vertical) or neutrons (horizontal). For convenience, an optional navigation map allows to jump directly in the region of interest. As the yield calculations proceed, the boxes corresponding to each nucleus are filled with 2 numbers characteristic of the calculation chosen by the user. By default these are the overall transmission and yield for each nucleus. The projectile and fragment chosen for the setting are indicated by a yellow and white strips respectively, ^{40}Ar and ^{28}O in the case of figure 7 (^{40}Ar is off screen in the figure). Right cliking on any of the nuclei opens a window displaying all the information for that nucleus.

The area located on the right of the chart of nuclides contains panes which displays the current settings of the fragment separator. Buttons located on each pane allow an easy access to the corresponding parameters. Other buttons located on top provide shortcuts to the most common tasks of the program, such as file opening and saving, etc.... Placing the mouse over any of those

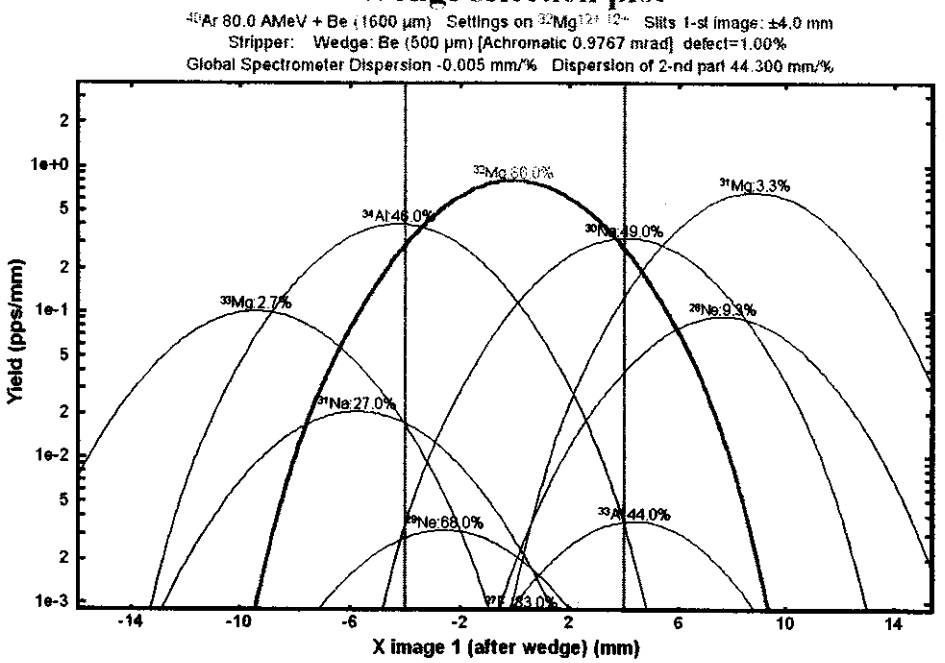

Fig. 8. Wedge selection plot showing the location of images corresponding to different nuclei at the achromatic focal plane. The slits are indicated as the two vertical lines.

buttons will prompt a small explanation box. Finally, the menu bar provides access to all the features of the program, with some redundancy to the buttons.

4.2 Configuration files

The program LISE can be used to calculate yields on any fragment separator very easily, using configuration files. These files contain all the information required to perform the calculations, i.e. primary beam characteristics, acceptances and optics coefficients. All parameters can be interactively modified and later saved as a new configuration saveset. The default configuration is for the fragment separator LISE, and standard configuration files for other fragment separators in the world are distributed with the program.

4.3 Outputs and plots

In addition to a standard output file containing all the informations about the current calculation, LISE can produce an extended number of plots showing different aspects of the phase space distributions as they occur along the fragment separator. As an example, figure 8 shows the images of various nuclei as they are calculated at the focal plane location. The slits are represented by

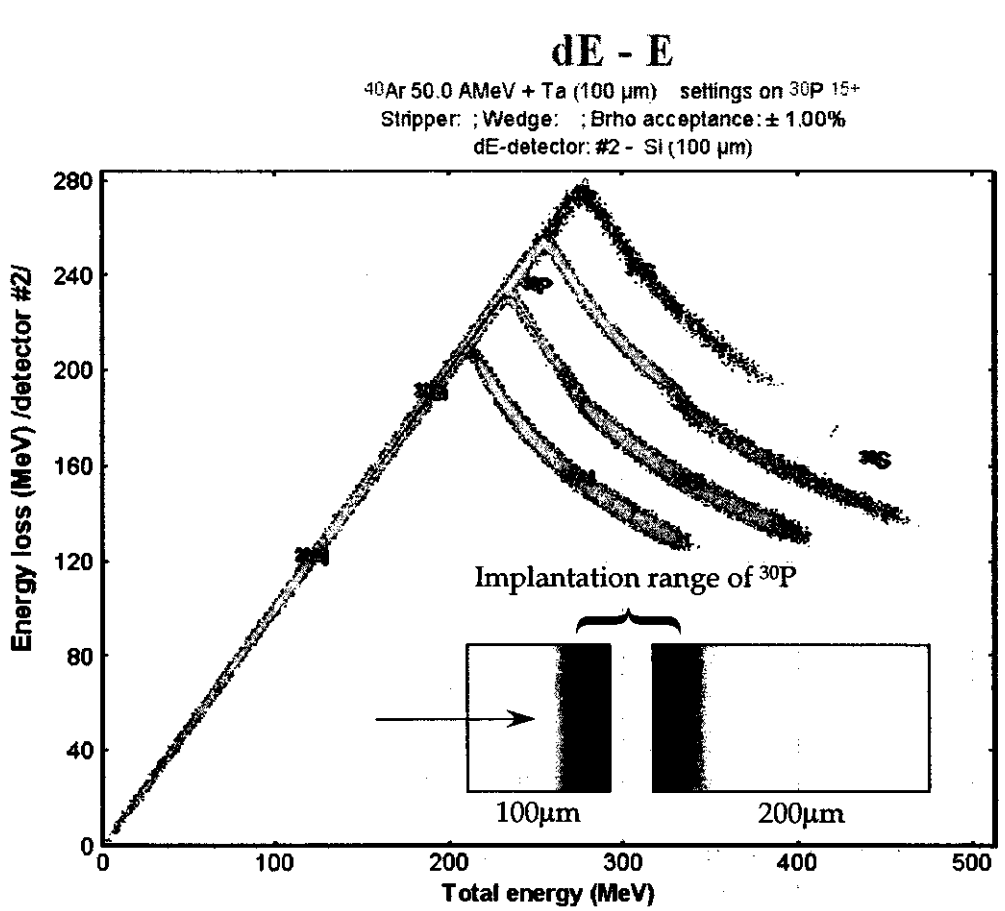

Fig. 9. Energy loss versus total energy plot for a few nuclei produced in the fragmentation of ^{40}Ar at 50 MeV/u. The desired fragment, ^{30}P, is implanted half in the 100 μm detector, half in the following 200 μm detector. The contaminants are implanted at different locations due to their different masses, charges and energies. Some of them completely punch through the 100 μm detector (^{27}Al, ^{28}Si, ^{29}P and ^{30}S).

two vertical lines and the vertical axis is in logarithmic scale as the yields differ by several orders of magnitude. The plot shows that among the fragments produced from the ^{40}Ar beam, only nuclei in the vicinity of ^{32}Mg are transmitted because their images end up at similar locations in the focal plane. As their number of protons and neutrons differs more and more from the chosen fragment, their images get shifted away from the slits and their transmissions (indicated in %) become smaller.

The full power of the Monte-Carlo generator already presented in earlier identification plots becomes apparent when calculating energy losses and ranges in foils of detectors. Figure 9 shows an example of energy loss versus total energy plot for nuclei being implanted between 2 Silicon detectors of thicknesses 100 μm and 200 μm. The energy loss in the 100 μm detector shows the characteristic inflexion point corresponding to the energy at which the nuclei are no longer implanted and punch through. Such a simulation is extremely useful

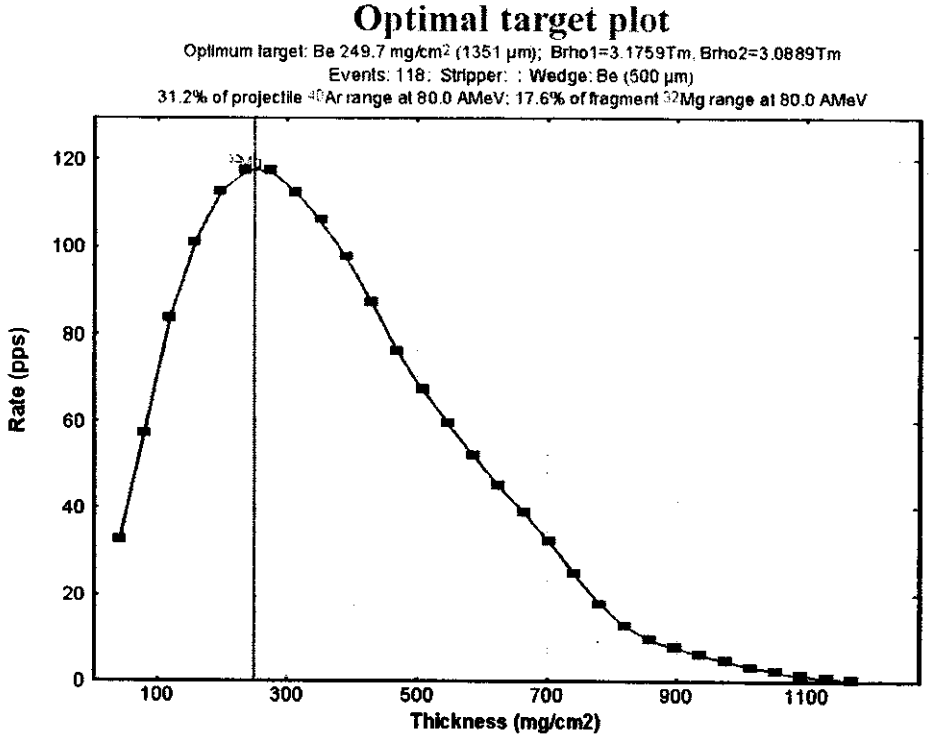

Fig. 10. Target optimization plot. An optimal target thickness of 250 mg/cm^2 is found at the maximum of the distribution.

in experiments where the implantation of a given nucleus has to be carefully adjusted.

4.4 Extra features and utilities

In this section we concentrate on the most important features only, as they are too numerous to be fully listed here.

4.4.1 Yield and transmission optimizations

One of the most important parameters the experimenter needs to determine prior to forecasting fragmentation yields is the target thickness. As the target thickness increases, the number of target nuclei interacting with the beam also increases, but so does the energy loss. In particular, the difference in energy loss between fragments produced from the front and the back of the target leads to a broadening of the momentum distribution which becomes rapidly much larger than most fragment separator momentum acceptances. As a result, the number of transmitted fragments decreases, and there is a thickness for which these two competing effects induce a maximum yield. This maximum depends

on the initial parameters of the primary beam and target used, as well as on the fragment chosen for optimization. Other effects such as straggling also increase with target thickness and limit the transmission. An example of a target thickness optimization calculated by LISE is shown on figure 10 in the case of ^{32}Mg produced from a primary beam of ^{40}Ar.

Once the optimum target thickness has been determined, the program can calculate the magnetic rigidity and velocity filter settings to transmit the desired fragment. In case a wedge is being used or other materials (such as detectors) are inserted in the beam, the program adjusts the settings accordingly. These calculations can also be performed in a reverse manner, in which the user specifies a desired energy or magnetic rigidity, and asks the program to calculate the amount of material needed to reach it. This feature is especially useful in experiments where the nuclei need to be implanted at a specific thickness in a foil or a detector.

After the parameters of the fragment separator have been set, the program can calculate the transmission of any nucleus, based on the optics as well as the positions of the various slits located along the beam line. Any modification of these parameters automatically clears the transmission data which needs to be re-calculated.

4.4.2 Physical parameters calculator

It is often important to calculate various physical parameters such as energy, magnetic rigidity, energy loss, range, etc ... for a given ion, and deduce these quantities from each other. This is the purpose of the physical calculator in which the user can quickly determine energy losses, ranges and stragglings in any kind of material or composite at any location along the beam line. This feature is especially useful when planning implantation experiments where the nuclei of interest are stopped in a medium to be later studied (radioactive decays, nuclear magnetic moments, etc ...). The calculator also features "backward" energy loss and range calculations in which the initial energy necessary to obtain the desired final energy or range is backward calculated. It can also determine the required amount of a given material to slow down particles from initial to final energies. Figure 11 shows the physical calculator window. Various radio buttons allow to choose the method of calculation and which parameter is entered. The ion is selected on the top pane of the window, and calculations are performed in up to seven materials.

4.4.3 Reaction kinematics

Two-body reaction kinematics and Q-values can easily be calculated within the framework of LISE. Plots of the center-of-mass and laboratory scattering

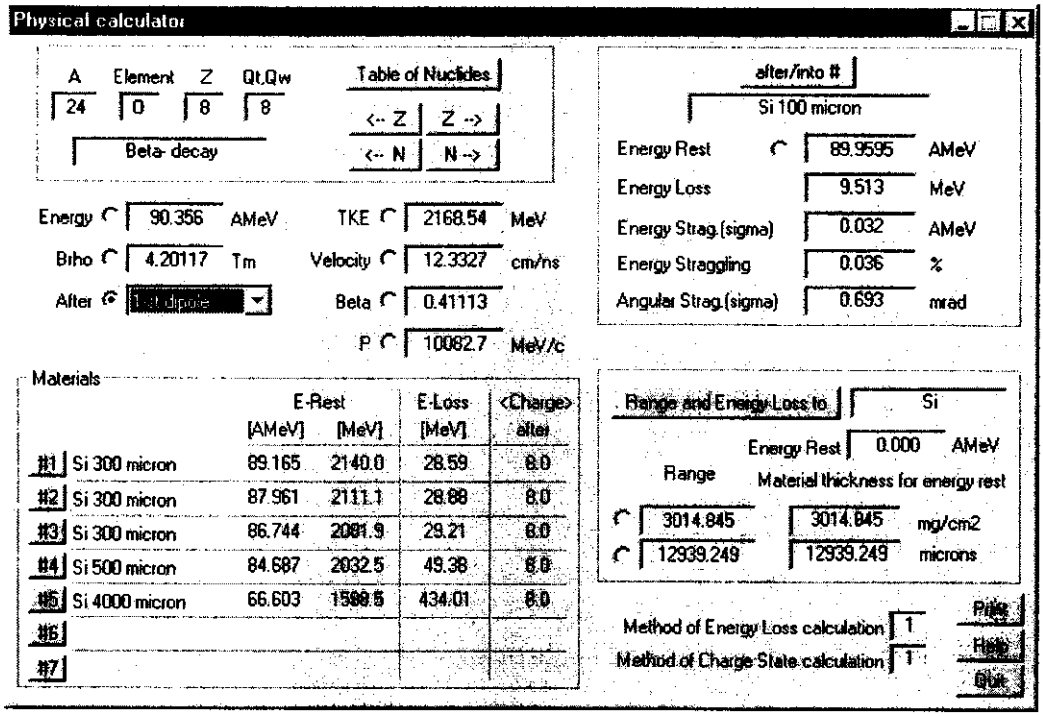

Fig. 11. Physical calculator window showing various calculations performed for the nucleus ^{24}O. The energy can be entered not only by the different parameters such as magnetic rigidity, velocity or momentum (radio buttons on the left), but also by specifying either an energy after a given material (top right) or the total range (bottom right).

angles versus energy can be produced and saved to disk. The calculations are fully relativistic.

4.5 Database

The program LISE has a built-in database which contains basic information on nuclei. It is based on the 1995 Atomic Mass Evaluation [34,35] for mass excess and related quantities, and other sources [36,37] for the half-lives. Plots of different quantities can easily be made as a function of atomic number Z, mass A, neutron number N or isospin $N - Z$. As for all monodimensional plots, the data can be saved to a file in ASCII format for use by an external program. Figure 12 shows an example of the database entry window. The user can quickly navigate through the table of nuclei using the atomic number and neutron number arrows. The database information is also included in the statistics window activated by right clicking on any nucleus directly on the table of nuclei display.

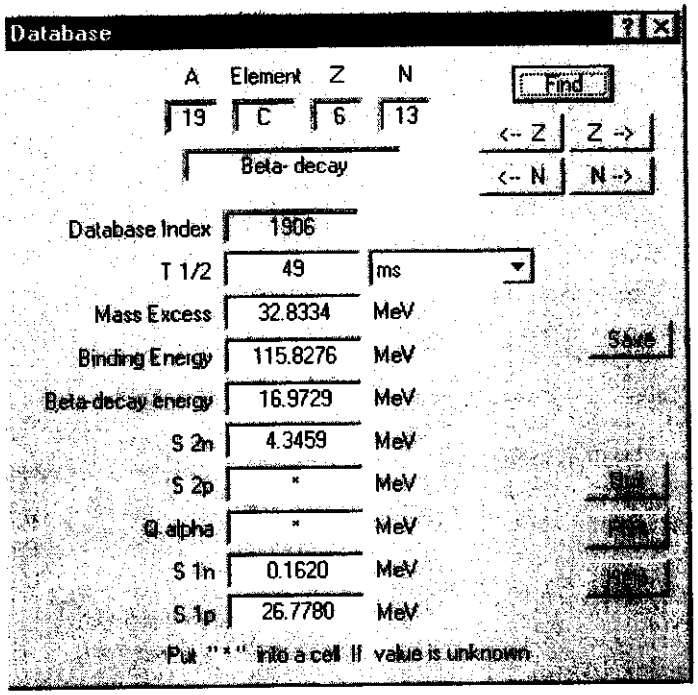

Fig. 12. Database entry window. See text for details.

4.6 On-line help

A fully featured on-line help is available, containing a table of contents as well as an index and search engine. The commands are explained in detail, both from the menu system and the toolbar. A history of changes in new versions is also included and describe the new features added since the beginning of the Windows^{TM} version. Finally, a reference manual provides additional information on the principle of the calculations, as well as a tutorial example to guide new users.

5 Comparison with data

As an example of the results and help provided by the program LISE during an experiment, we present a quantitative comparison with data obtained from the fragmentation of ^{86}Kr beams at 60 MeV/u on a composite Ni (100μm) and Be (500μm) target [38]. The particle identification in this experiment is complicated by the fact that the heaviest fragments emerge from the target with more than one charge state. Because the Bρ selection is sensitive to the charge of the ions, different mass and charge combinations of an isotopic line can get mixed on the regular energy loss vs. time-of-flight identification plot.

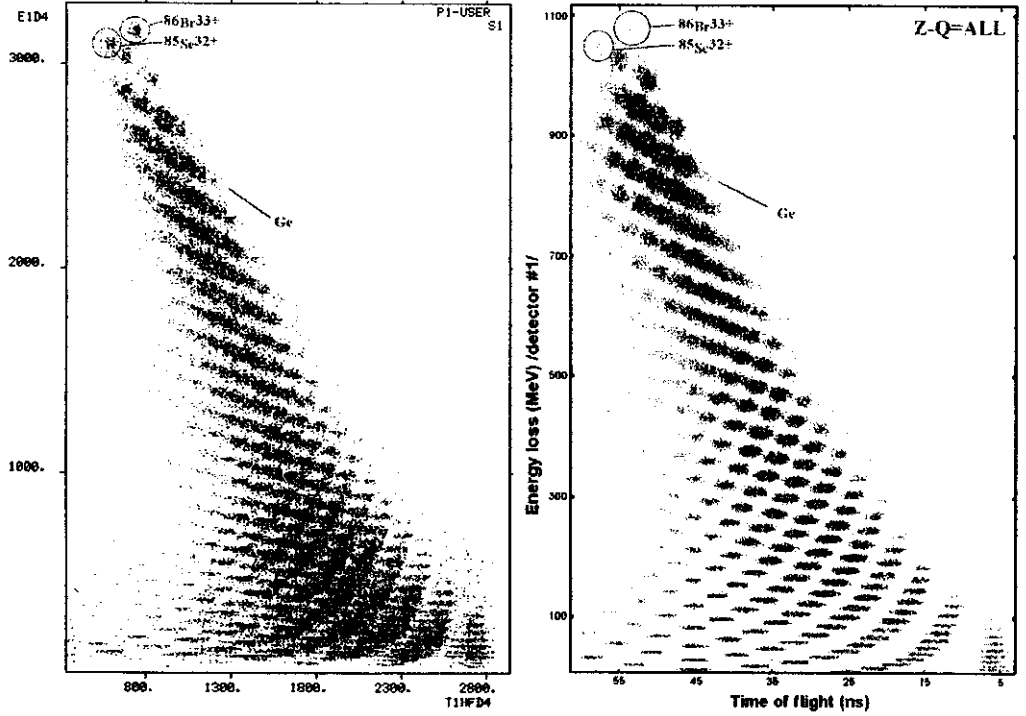

Fig. 13. Energy loss vs. time-of-flight identification plots. The spectrum on the left is the data taken during the experiment. The spectrum on the right is the LISE simulation. The isotopic lines between Cr and Ge clearly show different charge states and masses mixed together.

5.1 On-line identification

Figure 13 shows a qualitative comparison between the LISE calculation and the data taken at Bρ=2.367 T.m. The mixing of different masses and charge states is clearly visible for fragments between Cr and Ge. The lighter fragments appear to emerge fully stripped, and the A/Z=2 vertical line can be seen on the lower right corner of the spectra. To separate the different charge states, an additional measured parameter is necessary. Usually, the total kinetic energy of the fragments can be measured by stopping them in Silicon detectors. Then the charge state of each individual ion can be determined and used to gate the identification plot. Figure 14 shows the same comparison between calculation and data for the fully stripped ions only (Z-Q=0). The masses of isotopes between Cr and Ge are now clearly resolved.

The real power of the simulation is more apparent when an energy loss wedge is used to further select specific isotopes. As another example, we take the recent discovery of the doubly magic nucleus ^{48}Ni [39] for which a ^{58}Ni at 74.5 MeV/u projectile was used on a Ni target, followed by a Be wedge. Figure 15 shows the comparison between the experimental and calculated energy loss vs. time-of-flight spectra. Because only part of the usual "tree" pattern is visible,

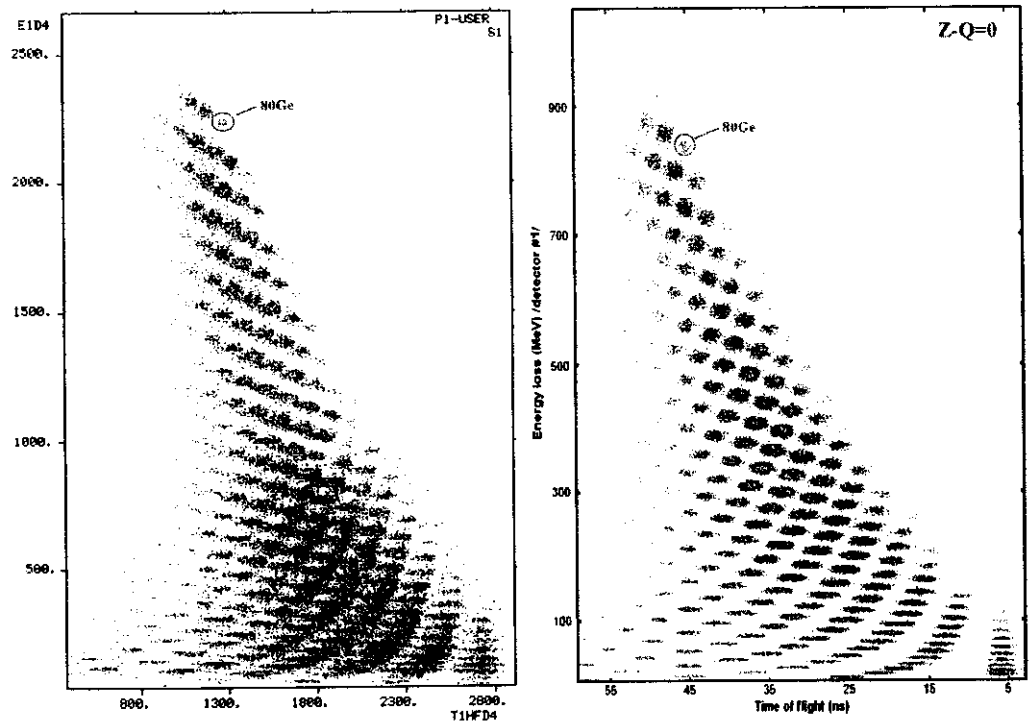

Fig. 14. Same as figure 13 but gated on the fully stripped ions. Now each mass can be clearly separated for the nuclei between Cr and Ge.

it is much more difficult to identify the group of events corresponding to a given nucleus. By comparing the data with the simulation though, this task becomes straightforward as the calculated pattern closely matches the data. The simulation proves to be especially useful in such a low yield experiment (less than one ^{48}Ni nucleus was produced per day) where it is essential to be able to verify that the settings of the fragment separator are correct without actually seeing the whole spectrum, only relying on the most produced nuclei to check the identification.

Note that both the time-of-flight and the energy loss can be calculated on an absolute scale, provided the flight path and detector thickness are known, and the experimental spectra are properly calibrated. In figure 15 the energy loss scale has been calibrated, and provide an additional check on the identification of the nuclei.

5.2 Yields

Figure 16 shows a quantitative comparison between the observed and calculated yields in the fragmentation of the ^{86}Kr beam at 60 MeV/u. The isotopic distributions are plotted for elements from Ti to Ge, for the fully stripped ions on the top and the hydrogen-like ions on the bottom. Overall the agreement

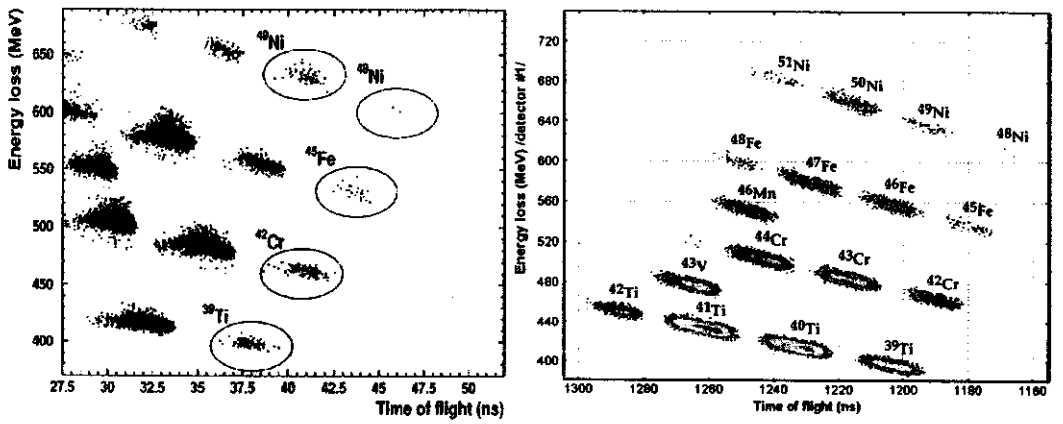

Fig. 15. Comparison between experimental and calculated identification plots. The spectrum on the left is taken from [39], and the spectrum on the right is the LISE simulation. The pattern observed in the experiment is readily recognized on the simulation, and makes the nucleus assignments straightforward.

is quite good, except in the case of Cu and Ge isotopes for which the absolute magnitude of the yields seems underestimated and overestimated respectively by a factor of 2 or so in the case of the fully stripped ions.

Note that contrary to the fully stripped ions, the yields of hydrogen-like ions decrease for smaller atomic numbers. This is due to the one electron charge state cross section which drops sharply as the Coulomb field of the nuclei decreases.

6 Conclusion

The program LISE described in this paper simulates the operation of fragment separators used to produce radioactive beams via projectile fragmentation. It can be used not only to forecast the yields and purity of radioactive beams, but also as an on-line tool for beam identification and tuning during experiments. Its interface and algorithms are designed to provide a user-friendly environment allowing easy adjustments of the input parameters and quick calculations. It can be configured to simulate fragment separators available in various research institutes by means of configuration files. As with any software product, the program LISE is constently updated and improved upon the requests of the users. It is readily available from the World Wide Web and runs on PC (Personal Computer) platforms, as well as Windows^{TM} emulators on other platforms such as Unix or MacOS^{TM}.

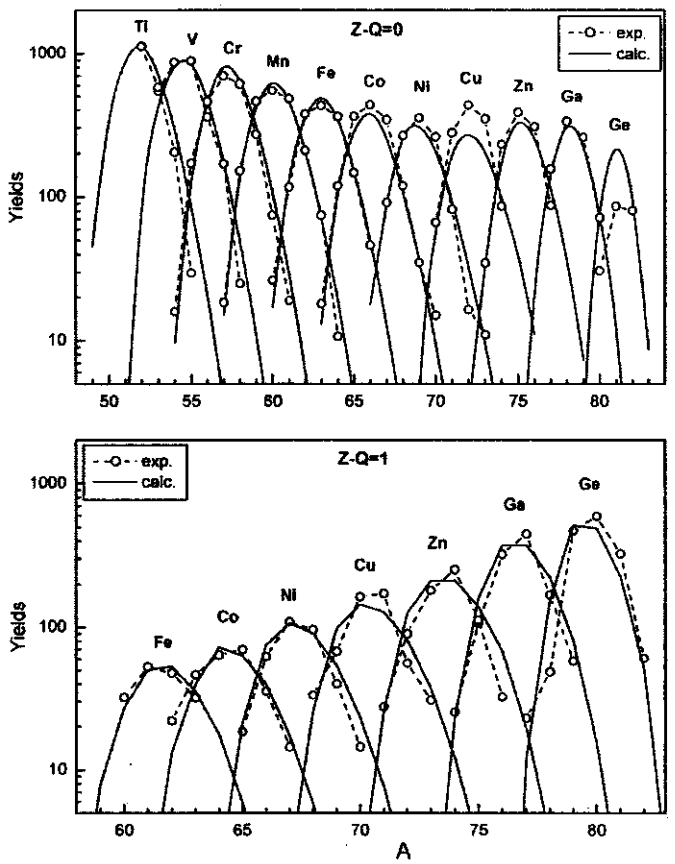

Fig. 16. Quantitative comparison between observed and calculated yields in the fragmentation of a ^{86}Kr beam at 60 MeV/u. The top figure shows the yields for fully stripped ions, and the bottom figure the yields for hydrogen-like ions.

7 Appendix

The three step fragmentation is obtained in the same way the two step was deduced. Knowing the number of fragments produced via a two step process from eq. 11, the same type of differential equation can be written:

$$\begin{aligned}\frac{\partial N3_{i,j,F}(x)}{\partial x} &= N2_{i,j}(x)\sigma_{j\to F} - N3_{i,j,F}(x)\sigma_F \\ &= (e^{-x\sigma_j}(e^{x(\sigma_j-\sigma_P)}(\sigma_j-\sigma_i) + e^{x(\sigma_j-\sigma_i)}(\sigma_P-\sigma_j) \\ &\quad +\sigma_i-\sigma_P)\sigma_{P\to i}\sigma_{i\to j})/((\sigma_j-\sigma_i)(\sigma_j-\sigma_P)(\sigma_i-\sigma_P)) * \sigma_{j\to F} \\ &\quad -N3_{i,j,F}(x)\sigma_F \qquad (22)\end{aligned}$$

where $\sigma_{i\to j}$ and $\sigma_{j\to F}$ are the cross sections for producing the intermediate fragment j from i and F from j respectively. The solution to this differential equation is the following:

$$N3_{i,j,F}(x) = \Big(e^{-x\sigma_F}\Big((-1+e^{x(\sigma_F-\sigma_i)})\sigma_j(\sigma_j-\sigma_P)\sigma_P+\sigma_F^2\Big(-e^{x(\sigma_F-\sigma_j)}\sigma_i+$$
$$e^{x(\sigma_F-\sigma_P)}(\sigma_i-\sigma_j)+e^{x(\sigma_F-\sigma_i)}\sigma_j-e^{x(\sigma_F-\sigma_i)}\sigma_P+e^{x\left(\sigma_F-\sigma_j\right)}\sigma_P\Big)+$$
$$\sigma_i^2\Big((-1+e^{x(\sigma_F-\sigma_P)})\sigma_j-\Big(-1+e^{x\left(\sigma_F-\sigma_j\right)}\Big)\sigma_P\Big)+\sigma_F\Big(e^{x\left(\sigma_F-\sigma_j\right)}\sigma_i^2-$$
$$e^{x(\sigma_F-\sigma_i)}\sigma_j^2+e^{x(\sigma_F-\sigma_P)}(-\sigma_i^2+\sigma_j^2)+e^{x(\sigma_F-\sigma_i)}\sigma_P^2-e^{x\left(\sigma_F-\sigma_j\right)}\sigma_P^2\Big)+$$
$$\sigma_i\Big(-(-1+e^{x(\sigma_F-\sigma_P)})\sigma_j^2+\Big(-1+e^{x\left(\sigma_F-\sigma_j\right)}\Big)\sigma_P^2\Big)\Big)\sigma_{P\to i}\sigma_{i\to j}\sigma_{j\to F}\Big)\Big/$$
$$((\sigma_F-\sigma_i)(\sigma_F-\sigma_j)(\sigma_i-\sigma_j)(\sigma_F-\sigma_P)(\sigma_i-\sigma_P)(\sigma_j-\sigma_P)) \qquad (23)$$

The total three step fragmentation yield is obtained by summing the individual yields over all possible paths to produce the final fragment:

$$N3_F = \sum_i \sum_{j<i} N3_{i,j,F} = \sum_{Z_i=Z_F}^{Z_P} \sum_{N_i=N_F}^{N_P} \sum_{Z_j=Z_F}^{Z_i} \sum_{N_j=N_F}^{N_i} N3_{i,j,F} \qquad (24)$$

References

[1] R. Anne, D. Bazin, A.C. Mueller, J.C. Jacmart, M. Langevin, Nucl. Instr. and Meth. **A257** (1987) 215-232.

[2] J.P. Dufour, R. Del Moral, H. Emmermann, F. Hubert, D. Jean, C. Poinot, M.S. Pravikoff, A. Fleury, H. Delagrange, K.-H. Schmidt, Nucl. Instr. and Meth. **A248** (1986) 267-281.

[3] K.-H. Schmidt, E. Hanelt, H. Geissel, G. Münzenberg, J.P. Dufour, Nucl. Instr. and Meth. **A260** (1987) 287-303.

[4] R. Anne and A.C. Mueller, Nucl. Instr. and Meth. **B70** (1992) 276-285.

[5] E.M. Friedlander and H.H. Heckmann, in *Treatise on Heavy Ion Science*, edited by D.A. Bromley (Plenum, New York, 1985) Vol. 1, p. 102.

[6] M. Bernas, S. Czajkowski, P. Armbruster, H. Geissel, P. Dessagne, C. Donzaud, H.-R. Faust, E. Hanelt, A. Heinz, M. Heese, C. Kozhuharov, C. Miehe, G. Münzenberg, M. Pfützner, C. Röhl, K.-H. Schmidt, W. Schwab, C. Stéphan, K. Sümmerer, L. Tassan-Got, B. Voss, Phys. Lett. **B331** (1994) 19-24.

[7] D. Bazin, D. Guerreau, R. Anne, D. Guillemaud-Mueller, A.C. Mueller, M.-G. Saint-Laurent, Nucl. Phys. **A515** (1990) 349-364.

[8] O.B. Tarasov, Yu.E. Penionzhkevich, R. Anne, D.S. Baiborodin, C. Borcea, Z. Dlouhy, D. Guillemaud-Mueller, A.S. Fomichev, R. Kalpakchieva, M. Lewitowicz, S.M. Lukyanov, V. Maidikov, A.C. Mueller, Yu.Ts. Oganessian, M.G. Saint-Laurent, N.K. Skobelev, O. Sorlin, V.D. Toneev, W. Trinder, Nucl. Phys. **A629** (1998) 605-620.

[9] K. Sümmerer, W. Brüchle, D.J. Morrissey, M. Schädel, B. Szweryn, Y. Weifan, Phys. Rev. **C42** (1990) 2546-2561.

[10] K. Sümmerer and B. Blank, Phys. Rev. **C61** (2000) 034607.

[11] Y. Yariv and Z. Fraenkel, Phys. Rev. **C20** (1979) 2227.

[12] W.A. Friedman, M.B. Tsang, D. Bazin and W.G. Lynch, MSU preprint MSUCL-1167, July 2000, to be published in Phys. Rev. C.

[13] D.J. Morrissey and B.M. Sherrill, Phil. Trans. R. Soc. Lond. A **356** (1998) 1985-2006.

[14] Y.P. Viyogi, T.J.M. Simons, P. Doll, D.E. Greiner, H.H. Heckman, D.L. Hendrie, P.J. Lindstrom, J. Mahoney, D.K. Scott, K. Van Bibber, G.D. Westfall, H. Wieman, H.J. Crawford, C. McParland, C.K. Gelbke, Phys. Rev. Lett. **42** (1979) 33-36.

[15] A.S. Goldhaber, Phys. Lett. **B53** (1974) 306-308.

[16] R. Dayras, A. Pagano, J. Barrette, B. Berthier, D.M. De Castro Rizzo, E. Chavez, O. Cisse, R. Legrain, M.C. Mermaz, E.C. Pollacco, H. Delagrange, W. Mittig, B. Heusch, R. Coniglione, G. Lanzano, A. Palmeri, Nucl. Phys. **A460** (1986) 299-323.

[17] K. Van Bibber, D.L. Hendrie, D.K. Scott, H.H. Weiman, L.S. Schroeder, J.V. Geaga, S.A. Cessin, R. Treuhaft, Y.J. Grossiord, J.O. Rasmussen, C.Y. Wong, Phys. Rev. Lett. **43** (1979) 840-844.

[18] D.J. Morrissey, Phys. Rev. **C39** (1989) 460.

[19] W.A. Friedman, Phys. Rev. **C27** (1983) 569.

[20] LISE parametrization, to be published.

[21] V. Borrel, D. Guerreau, J. Galin, B. Gatty, D. Jacquet, X. Tarrago, Z. Phys. **A314** (1983) 191.

[22] F. Rami, J.P. Coffin, G. Guillaume, B. Heusch, P. Wagner, A. Fahli, P. Fintz, Nucl. Phys. **A444** (1985) 349.

[23] N. Iwasa, H. Geissel, G. Münzenberg, C. Scheidenberger, T. Schwab, H. Wollnik, Nucl. Instr. and Meth. **B126** (1997) 284-289.

[24] D. Bazin and B. Sherrill, Phys. Rev. **E50** (1994) 4017-4021.

[25] K.L. Brown D.C. Carey, C. Iselin, F. Rothacker, Transport: a computer program for designing charged particles beam transport systems, CERN 80-04 (1980).

[26] F. Hubert, R. Bimbot, H. Gauvin , Atom. Data and Nucl. Data Tables **46** (1990) 1-213.

[27] L.C. Northcliffe and R.F. Schilling, Nucl. Dat. Tabl. **A7** (1970) 233.

[28] J. F. Ziegler et al., "The Stopping and Range of Ions in Solids", Pergamon Press, New York, 1985.

[29] D. Guillemaud-Mueller, M.O. Lampert, D. Pons, M. Langevin, IEEE Trans. on Nucl. Science, Vol. 33, No. 1 (1986) 343-345.

[30] R. Anne, J. Herault, R. Bimbot, H. Gauvin, G. Bastin, F. Hubert, Nucl. Instr. and Meth. **B34** (1988) 295-308.

[31] J.A. Winger, B.M. Sherrill, D.J. Morrissey, Nucl. Instr. and Meth. **B70** (1992) 380-392.

[32] A. Leon, S. Melki, D. Lisfi, J.P. Grandin, P. Jardin, M.G. Suraud, A. Cassimi, Atom. Data and Nucl. Data Tables **69** (1998) 217-238.

[33] K. Shima, T. Ishihara, T. Mikumo, Nucl. Instr. and Meth. **200** (1982) 605-608.

[34] G. Audi and A.H. Wapstra, Nucl. Phys. **A595** (1995) 409-480;

[35] G. Audi and A.H. Wapstra, Nucl. Phys. **A565** (1993) 1.

[36] G. Pfennig, H. Klewe-Nebenius, W. Seelmann-Eggeberg, "Chart of the Nuclides", 6^{th} edition (1995), printed by Druckhaus, Haberbeck GmbH, D-32791 Lage/Lippe.

[37] J.K. Tuli, Brookhaven National Laboratory, P.O. Box 5000, Upton, NY 11973-5000, USA.

[38] J.M. Daugas, R. Grzywacz, M. Lewitowicz, L. Achouri, J.C. Angelique, D. Baiborodin, K. Bennaceur, R. Bentida, R. Beraud, C. Borcea, C. Bingham, W.N. Catford, A. Emsallem, G. de France, H. Grawe, K.L. Jones, R.C. Lemmon, M.J. Lopez-Jimenez, F. Nowacki, F. de Oliveira Santos, M. Pfützner, P.H. Regan, K. Rykaczewski, J.E. Sauvestre, M. Sawicka, G. Sletten, M. Stanoiu, Phys. Lett. **B476** (2000) 213.

[39] B. Blank, M. Chartier, S. Czajkowski, J. Giovinazzo, M.S. Pravikoff, J.-C. Thomas, G. de France, F. de Oliveira Santos, M. Lewitowicz, C. Borcea, R. Grzywacz, Z. Janas, M. Pfützner, Phys. Rev. Lett. **84** (2000) 1116-1119.